

Analysis of laminar and turbulent natural, mixed and forced convection in cavities by heatlines

I. HERNÁNDEZ-LÓPEZ^{1),2)}, J. XAMÁN¹⁾, G. ÁLVAREZ¹⁾,
Y. CHÁVEZ¹⁾, J. ARCE¹⁾

¹⁾ *Centro Nacional de Investigación y Desarrollo Tecnológico
CENIDET-TecNM-SEP
Prol. Av. Palmira S/N. Col. Palmira. Cuernavaca,
Morelos, CP. 62490, México
e-mails: jxaman@cenidet.edu.mx, gaby@cenidet.edu.mx,
ycchena@cenidet.edu.mx, jesuso@cenidet.edu.mx*

²⁾ *Instituto Tecnológico de Zacatepec. ITZ-TecNM-SEP
Calzada Tecnológico No. 27, Zacatepec de Hidalgo,
Morelos, CP 62780, México
e-mail: ihernan@cenidet.edu.mx*

LAMINAR AND TURBULENT CONVECTIVE HEAT TRANSFER in a ventilated and non-ventilated cavity was analyzed by heatlines. Heatlines show that in non-ventilated cavities it is possible to estimate the energy path using the streamlines for turbulent flow regime. In ventilated cavities, heatlines allow to observe that thermal energy travels along the top, by the bottom or by both paths due to the inertial force, the buoyant force or a combination of both, respectively. In the laminar regime, these situations are well established for the Rayleigh number (Ra). Nevertheless, in the turbulent regime, it was found that the combined effect of the inertial and buoyant forces on the energy path is disrupted when $Ra > 10^9$. Furthermore, heatlines in conjunction with temperature and velocity profiles allow to see that natural convection is preferred when cooling is required, while the forced convection is a better choice if heating is needed.

Key words: heatlines; natural, mixed and forced convection.

Copyright © 2016 by IPPT PAN

Notations

$C_{1\varepsilon}, C_{2\varepsilon}, C_{3\varepsilon}, C_\mu$	coefficients of the turbulence model,
C_p	specific heat, $\text{J kg}^{-1} \text{K}^{-1}$,
G_k	buoyancy production/destruction of kinetic energy,
g	gravity acceleration, $9.81 \text{ m} \cdot \text{s}^{-2}$,
H	heat function,
H^*	dimensionless heat function ($H/\Gamma_T \Delta T$),
\mathbf{J}	thermal energy flow vector per unit area, $\text{W} \cdot \text{m}^{-2}$,
k	turbulence kinetic energy, $\text{m}^2 \cdot \text{s}^{-2}$,
L	length and height of the cavity, m,

L_a	distance of the opening, m,
\mathbf{n}	normal unit vector,
Nu	average Nusselt number,
P	pressure, $\text{N} \cdot \text{m}^{-2}$,
P_k	production of turbulent kinetic energy,
Pr	Prandtl number ($\mu C_p / \lambda$),
q	heat flux, $\text{W} \cdot \text{m}^{-2}$,
Ra	Rayleigh number ($\rho g \beta \Delta T L^3 / \mu \alpha$),
Re	Reynolds number ($\rho U_{in} L / \mu$),
T	temperature, K,
T^*	dimensionless temperature $(T - T_C / T_H - T_C)$,
T_0	average temperature $(T_H + T_C / 2)$,
U_{in}	inlet velocity ($\text{Re} \mu / \rho L$),
U_0	buoyancy reference velocity $(g \beta \Delta T L)^{0.5}$,
u, v	horizontal and vertical velocities, $\text{m} \cdot \text{s}^{-1}$,
u^*, v^*	dimensionless horizontal and vertical velocity components $(u / U_0, v / U_0)$,
x, y	dimensional coordinates, m,
x^*, y^*	dimensionless coordinates $(x / L, y / L)$.

Greek symbols

α	thermal diffusivity, $\text{m}^2 \cdot \text{s}^{-1}$,
β	thermal expansion coefficient, K^{-1} ,
ΔT	temperature difference $(T_H - T_C)$,
ε	rate of dissipation of k , $\text{m}^2 \cdot \text{s}^{-3}$,
λ	thermal conductivity, $\text{W} \cdot \text{m}^{-1} \cdot \text{K}^{-1}$,
μ	dynamic viscosity, $\text{kg} \cdot \text{m}^{-1} \cdot \text{s}^{-1}$,
μ_t	turbulent viscosity, $\text{kg} \cdot \text{m}^{-1} \cdot \text{s}^{-1}$,
ρ	density, $\text{kg} \cdot \text{m}^{-3}$,
σ_k	Prandtl number for k ,
σ_ε	Prandtl number for ε ,
σ_T	Prandtl number for T ,
ψ	stream function,
ψ^*	dimensionless stream function $(\psi / U_0 L)$.

Subscripts

<i>conv</i>	convective,
<i>in</i>	inlet,
<i>ref</i>	reference for calculating the heat function.

1. Introduction

GENERALLY, IN TRANSPORT PHENOMENA, the study of the behavior of the variables is carried out with isolines, while in fluid flows, it is common to use streamlines to visualize flow fields. In conduction heat transfer problems where the heat flux is perpendicular to the isothermals, isotherms are used for the analysis of results. However, heat transfer by convection involves a combination of both heat diffusion and advection of thermal energy, which makes convection a more complex phenomenon than conduction. This complexity has led the scientific community to draw upon streamlines and isothermals for interpreta-

tion and discussion of results of problems involving heat convection. However, isotherms and streamlines only provide the temperature field and the path of the fluid flow, respectively. If the interest lies in knowing the path of the thermal energy, it is necessary to analyze the isotherms and the streamlines to estimate the heat flux path; this situation may lead to misinterpretations of the results in problems that are highly advective, because the energy flow is not necessarily perpendicular to the isothermals in this type of problems.

To overcome this limitation in the analysis of convective energy transport, Kimura and Bejan proposed a visualization tool for two-dimensional flows that allows to observe the actual path of the thermal energy flow [1], taking into account the diffusive and advective contributions. From the energy equation, and using an equivalent development to the deduction of the stream function, the authors mathematically defined the heat function. The isolines of the heat function are called heatlines, and they are the appropriate tool to visualize the path of thermal energy. The authors obtained a *Poisson-type* equation which was solved numerically in order to get the heatlines. In a later work, Aggarwal and Manhapra determined the heat function by direct integration of the equations that define it [2]. Therefore, the authors concluded that the iterative solution of the Poisson equation method is not necessary. Zhao *et al.* showed that similar results are obtained if the heat function is determined by the Poisson equation method or by the direct integration method [3]. The authors also concluded that the convergence errors are different for the two different methods. Recently, Biswal and Basak found that the magnitudes of heat functions change drastically with the selection of the location of the heat function data. Nevertheless, the heat flux patterns remain the same irrespective of the heat function boundary conditions [4]. In heat transfer by convection, many studies on rectangular cavities have used heatlines for the interpretation and analysis of results. Such studies include natural convection problems [5–8], mixed convection [9, 10] and conjugated heat transfer [11–13]. However, all these studies were developed for laminar flow regime problems. In turbulent regime flow, only two studies on convective heat transfer problems have used heatlines. One study concerns the turbulent natural convection problem of a plane plate dissipating heat to the environment [14], and the second one is a study of cooling in a gas turbine [15]. Nevertheless, it is important to apply Bejan’s heatlines to systems involving turbulent flow regime which is present in such an important daily processes as ventilation of buildings. The knowledge of the actual path of the thermal energy flow can help to improve the bioclimatic building design and passive solar systems.

Therefore, the purpose of this work is to analyze and visualize the results in laminar and turbulent forced, mixed and natural convection in closed and ventilated square cavities by using heatlines. Thereby, for the first time it will

be possible to depict the path of the thermal energy inside cavities with turbulent flow using heatlines. In order to handle this situation, two problems are considered. The first problem studies the heat transfer by natural convection in a square cavity heated on the vertical walls. The second problem studies the convection heat transfer in a ventilated cavity. In the latter problem, three cases are analyzed: (i) forced convection ($Ri = 0.1$), (ii) mixed convection ($Ri = 1$) and (iii) natural convection ($Ri = 10$).

2. Physical model

The steady state convective heat transfer in a square cavity is considered. The cavity, with the length L , is filled with air ($Pr = 0.71$). In order to establish two-dimensional flow, the dimension in “ z ” direction is supposed to be much longer than dimensions in “ x ” and “ y ” directions. Air inside the cavity is considered as a continuum, isotropic and homogeneous medium that behaves as a Newtonian and incompressible fluid. On the other hand, the medium is affected only by the gravitational field acting in “ y ” negative direction. Finally, physical properties are considered independent of pressure and temperature, except for the density in the buoyancy term, where the Boussinesq approximation is used.

2.1. Physical model of the closed cavity

The enclosure was modeled as a closed cavity heated differentially in the horizontal direction as shown in Fig. 1a. The temperature on the left vertical wall (T_H) is higher than on the right vertical wall (T_C), whereas the upper and lower horizontal walls are adiabatic. On the wall surfaces, non-slip condition prevails, so the velocity components are equal to zero on all of them.

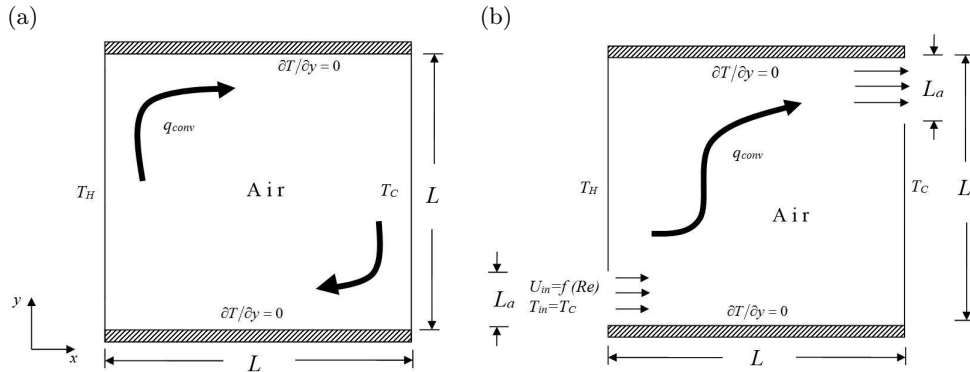


FIG. 1. Physical model: (a) closed cavity and (b) ventilated cavity.

2.2. Physical model of the ventilated cavity

The ventilated cavity has two openings. The inlet is located on the bottom side of the left vertical wall. The outlet is located on the top side of the right vertical wall. The dimensions of the openings are L_a , where $L = 10L_a$. Moreover, air flow enters at the velocity U_{in} and temperature $T_{in} = T_C$, which is equal to the temperature surface of the right vertical wall, which, in turn, is at a lower temperature than the left vertical wall. Figure 1b shows the physical model of the ventilated cavity.

3. Mathematical model

3.1. Governing equations

The governing equations for the turbulent convective heat transfer in a steady state are the conservation equations of mass, momentum and energy averaged in time. These equations are given below:

$$(3.1) \quad \frac{\partial(\rho u_i)}{\partial x_i} = 0,$$

$$(3.2) \quad \frac{\partial(\rho u_i u_j)}{\partial x_j} = -\frac{\partial P}{\partial x_j} + \frac{\partial}{\partial x_j} \left(\mu \frac{\partial u_i}{\partial x_j} - \overline{\rho u'_i u'_j} \right) - \rho g_i \beta (T - T_o),$$

$$(3.3) \quad \frac{\partial(\rho u_i T)}{\partial x_i} = \frac{\partial}{\partial x_i} \left(\frac{\lambda}{C_p} \frac{\partial T}{\partial x_i} - \overline{\rho u'_i T'} \right).$$

For the laminar flow, it is clear that both the Reynolds stress tensor and the turbulent heat flux vector are null:

$$(3.4) \quad \overline{\rho u'_i u'_j} = 0,$$

$$(3.5) \quad \overline{\rho u'_i T'} = 0.$$

In the case of turbulent flow, the Reynolds stress tensor is determined by the Boussinesq hypothesis, whereas the turbulent heat flux vector is obtained applying the Reynolds analogy. This way, the Reynolds stress tensor and the turbulent heat flux vector are modeled using the following mathematical expressions:

$$(3.6) \quad \overline{\rho u'_i u'_j} = -\mu_t \left(\frac{\partial u_i}{\partial x_j} + \frac{\partial u_j}{\partial x_i} \right) + \frac{2}{3} \rho k \delta_{ij},$$

$$(3.7) \quad \overline{\rho u'_i T'} = -\frac{\mu_t}{\sigma_t} \frac{\partial T}{\partial x_i}.$$

On the other hand, the turbulent viscosity is computed as

$$(3.8) \quad \mu_t = C_\mu \frac{\rho k^2}{\varepsilon}.$$

Finally, to close the system of equations, it is necessary to include the equations of turbulent kinetic energy transport and turbulent kinetic energy dissipation:

$$(3.9) \quad \frac{\partial(\rho u_i k)}{\partial x_i} = \frac{\partial}{\partial x_i} \left[\left(\mu + \frac{\mu_t}{\sigma_k} \right) \frac{\partial k}{\partial x_i} \right] + P_k + G_k - \rho \varepsilon,$$

$$(3.10) \quad \frac{\partial(\rho u_i \varepsilon)}{\partial x_i} = \frac{\partial}{\partial x_i} \left[\left(\mu + \frac{\mu_t}{\sigma_\varepsilon} \right) \frac{\partial \varepsilon}{\partial x_i} \right] + [C_{1\varepsilon}(P_\varepsilon + G_\varepsilon + C_{3\varepsilon}) - C_{2\varepsilon}\rho\varepsilon] \frac{\varepsilon}{k}.$$

where P_k and G_k are the shearing production and the generation/destruction of buoyancy turbulent kinetic energy. The values of the coefficients for the turbulence model are $C_\mu = 0.09$, $C_{1\varepsilon} = 1.44$, $C_{2\varepsilon} = 1.92C_{1\varepsilon} = \tanh v/u$, $\sigma_k = 1.0$ and $\sigma_\varepsilon = 1.3$ [16].

3.2. Boundary conditions

Based on the no-slip condition, the velocity components over the wall surfaces are null. Furthermore, the thermal boundary conditions are $\partial T/\partial y = 0$ for the adiabatic boundaries, whereas the temperatures for the isothermal walls are $T = T_H = 300$ K (27°C) and $T = T_C = 288$ K (15°C) for $x = 0$ and $x = L$, respectively. The boundary conditions for the turbulence model are $k = 0$ and $\varepsilon = \infty$. According to [16], the boundary condition for ε can be assigned as a large numerical value. In this study it was $\varepsilon = 100$. Additionally, for the case of ventilated cavity the following assumptions were considered: $u = U_{in} = f(\text{Re})$, $T = T_{in} = T_C$, $k_{in} = 1.5(0.04U_{in})^2$ and $\varepsilon_{in} = (k_{in})^{1.5}/(0.1L_{in})$ at the air inlet zone; open boundary conditions for all the variables at the air outlet zone were considered as $\partial\phi/\partial x = 0$ ($\phi = \text{variable}$).

3.3. Heat function equation

According to [1], equations (3.11) and (3.12) define the heat function for heat convection problems in the laminar flow regime as follows:

$$(3.11) \quad \frac{\partial H}{\partial x} = -\rho v(T - T_{ref}) + \frac{\lambda}{C_p} \frac{\partial T}{\partial y},$$

$$(3.12) \quad \frac{\partial H}{\partial y} = \rho u(T - T_{ref}) - \frac{\lambda}{C_p} \frac{\partial T}{\partial x}.$$

Also, we develop a Poisson-type equation from Eqs. (3.11) and (3.12) to numerically determine the heat function:

$$(3.13) \quad (3.13) \quad \frac{\partial}{\partial x} \left(\frac{C_p}{\lambda} \frac{\partial H}{\partial x} \right) + \frac{\partial}{\partial y} \left(\frac{C_p}{\lambda} \frac{\partial H}{\partial y} \right) + \frac{\partial}{\partial x} \left[\frac{\rho C_p v}{\lambda} (T - T_{ref}) \right] - \frac{\partial}{\partial y} \left[\frac{\rho C_p u}{\lambda} (T - T_{ref}) \right] = 0.$$

With Eqs. (3.11) and (3.12) it is possible to obtain the heat function by the method of integration, while using Eq. (3.13), the heat function is obtained by solving the Poisson equation.

In order to determine the relationships that define the heat function in turbulent flow, it is necessary to start from the energy equation in its form averaged in time for two dimensions and at a temperature ($T - T_{ref}$):

$$(3.14) \quad \frac{\partial(\rho u T)}{\partial x} + \frac{\partial(\rho v T)}{\partial y} = \frac{\partial}{\partial x} \left(\frac{\lambda}{C_p} \frac{\partial T}{\partial x} - \overline{\rho u'(T' - T_{ref})} \right) + \frac{\partial}{\partial y} \left(\frac{\lambda}{C_p} \frac{\partial T}{\partial y} - \overline{\rho v'(T' - T_{ref})} \right),$$

where, according to equation (3.7), the turbulent heat flux can be modeled as

$$(3.15) \quad \overline{\rho u'_i(T' - T_{ref})} = -\frac{\mu_t}{\sigma_t} \frac{\partial T}{\partial x_i}.$$

In this way, substituting Eq. (3.15) into Eq. (3.14) and after some mathematical manipulation and rearrangement of terms we obtain the following:

$$(3.16) \quad \frac{\partial}{\partial x} \left[\rho u(T - T_{ref}) - \left(\frac{\lambda}{C_p} + \frac{\mu_t}{\sigma_t} \right) \frac{\partial T}{\partial x} \right] + \frac{\partial}{\partial y} \left[\rho v(T - T_{ref}) - \left(\frac{\lambda}{C_p} + \frac{\mu_t}{\sigma_t} \right) \frac{\partial T}{\partial y} \right] = 0.$$

This equation allows to define the arguments of the derivatives as the components of thermal energy flow per unit area:

$$(3.17) \quad J_i = \rho u_i(T - T_{ref}) - \Gamma_T \frac{\partial T}{\partial x_i},$$

where $\Gamma_T = \left(\frac{\lambda}{C_p} + \frac{\mu_t}{\sigma_t} \right)$ is the effective diffusive property for T .

Thus, Eq. (3.16) can be expressed as

$$(3.18) \quad \frac{\partial J_x}{\partial x} + \frac{\partial J_y}{\partial y} = 0.$$

Moreover, based on Fig. 2, the thermal energy flux passing through a control surface element dA can be determined as

$$(3.19) \quad dH = \mathbf{J} \cdot \mathbf{n} dA.$$

Since the flow is two-dimensional, the surface differential element is $ds \times 1$; therefore we obtain

$$(3.20) \quad dH = \mathbf{J} \cdot \mathbf{n} ds$$

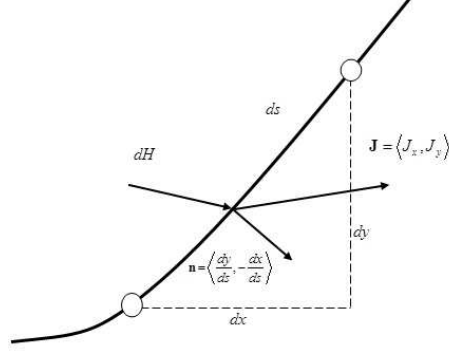


FIG. 2. Differential element of a heatline to determine the heat function.

leading to

$$(3.21) \quad dH = -J_y dx + J_x dy.$$

Besides, taking into account the definition of the total derivate, the differential of the heat function can be expressed as

$$(3.22) \quad dH = \left(\frac{\partial H}{\partial x} \right) dx + \left(\frac{\partial H}{\partial y} \right) dy.$$

Thus, analyzing Eqs. (3.21) and (3.22) it is found that

$$(3.23) \quad \frac{\partial H}{\partial x} = -J_y,$$

$$(3.24) \quad \frac{\partial H}{\partial y} = J_x.$$

This way, the relationships that define the heat function for the turbulent flow regime are:

$$(3.25) \quad \frac{\partial H}{\partial x} = -\rho v(T - T_{ref}) + \Gamma_T \frac{\partial T}{\partial y},$$

$$(3.26) \quad \frac{\partial H}{\partial y} = \rho u(T - T_{ref}) - \Gamma_T \frac{\partial T}{\partial x}.$$

In order to determine the Poisson equation, Eqs. (3.25) and (3.26) are divided by the effective diffusive property, derived with respect to the corresponding direction and finally added to both equations [17, 18]:

$$(3.27) \quad \frac{\partial}{\partial x} \left(\frac{1}{\Gamma_T} \frac{\partial H}{\partial x} \right) + \frac{\partial}{\partial y} \left(\frac{1}{\Gamma_T} \frac{\partial H}{\partial y} \right) + \frac{\partial}{\partial x} \left[\frac{\rho v}{\Gamma_T} (T - T_{ref}) \right] - \frac{\partial}{\partial y} \left[\frac{\rho u}{\Gamma_T} (T - T_{ref}) \right] = 0.$$

4. Methodology of solution and verification

The governing equations of fluid flow and heat transfer, as well as the equation of the heat function (Eqs. 3.25–3.27), were solved numerically using the finite volume method [19]. In order to implement the numerical algorithm, the mathematical model was represented by the convection-diffusion general equation:

$$(4.1) \quad \frac{\partial}{\partial x_i}(\rho u_i \phi) = \frac{\partial}{\partial x_i} \left(\Gamma \frac{\partial \phi}{\partial x_i} \right) + S_\phi.$$

This equation was integrated over the corresponding control volume, which generated a system of algebraic equations that can be summarized in the following expression:

$$(4.2) \quad a_P \phi_P^{n+1} = \sum_{nb=E,W,N,S} a_{nb} \phi_{nb}^{n+1} + b^n,$$

where ϕ is the variable to be discretized over the control volume, n is the number of the iteration, nb are the coefficients of the nodes neighbor to the node of interest and b is the source term.

A stretching function was used to intensify the number of computational nodes over the regions close to the walls in order to include the boundary layer. The velocity components were computed on a staggered grid whereas the scalar variables were located on the main grid. The coupling between the equations of momentum and continuity was carried out using the SIMPLEC algorithm [20]. The central scheme was used for the diffusive terms whereas the hybrid scheme was used for the convective terms. The resulting system of equations was solved using the line by line Gauss–Seidel method with alternating directions (LGS-ADI). The convergence criterion was set as 10^{-10} for each equation; additionally, under-relaxation was introduced using a false transient formulation.

In order to verify the numerical codes, a benchmark problem was reproduced. This problem is a differentially heated cavity reported in the literature for both laminar and turbulent flow [21–24]. Table 1 shows the comparison of results obtained for laminar and turbulent flow regimes. For the laminar flow regime, the percentage differences are below 4.06%. For the turbulent flow, the maximum percentage difference is 3.43%, which corresponds to the case of $\text{Ra} = 10^9$. Thus, based on these results, it can be considered that both codes provide acceptable results.

A numerical subroutine in FORTRAN was developed to calculate the heat function for the problem of the differentially heated cavity in the laminar flow regime using the integration and the Poisson equation methods (Eqs. 3.11–3.13).

Table 1a. Comparison of the average Nusselt number obtained from the studies reported in laminar flow regime.

Ra	De Vahl Davis [21]	Markatos [23]	Fusegi [22]	Barakos et al. [24]	Present work
10^3	1.117 (0.09)	1.108 (0.01)	1.105 (1.17)	1.114 (0.35)	1.118
10^4	2.238 (0.45)	2.201 (2.13)	2.203 (2.04)	2.245 (0.13)	2.248
10^5	4.509 (0.84)	4.430 (0.60)	4.646 (4.06)	4.510 (1.17)	4.457
10^6	8.817 (0.54)	8.754 (1.26)	9.012 (1.61)	8.806 (0.66)	8.865

Note: values in ‘ () ’ are the corresponding percentage differences

Table 1b. Comparison of the average Nusselt number obtained from the studies reported in turbulent flow regime.

Ra	Markatos [23]	Henkes [16]	Barakos <i>et al.</i> [24]	Present work
10^9	74.957 (0.82)	58.510 (0.81)	60.100 (3.43)	58.033
10^{10}	159.887 (0.01)	137.500 (0.09)	134.600 (2.24)	137.626
10^{11}	341.046 (0.75)	320.960 (0.75)	—	318.539
10^{12}	727.468 (2.57)	744.680 (2.56)	—	725.571

Note: values in ‘ () ’ are the corresponding percentage differences

Figure 3 shows a good agreement in the qualitative comparison of the heat function for both methods. Quantitatively, the largest percentage difference was approximately 3%, which corresponds to the case $Ra = 10^6$. These results allow us to assure that the two methods provide acceptable heatlines, with the only difference that the Poisson equation method requires more computational time for processing an iterative solution. Therefore, based on these results, the integration method was chosen for verification. In order to verify the subroutine, the values of the heatlines were compared to the results obtained by [12]. Table 2 shows the comparison of the maximum value for the heatline corresponding to $Ra = 10^3$ – 10^6 , where the maximum percentage difference was 0.70%. According to the advantages of the integration method mentioned above (Eqs. 3.25–3.26), this method was used to compute the heatlines in all the cases of turbulent regime flow (what is the main contribution of this work).

Table 2. Comparison of the maximum heatline for the problem of the differentially heated cavity in laminar flow regime.

Ra	Deng and Tang [12]	Present work	Δ
10^3	1.118	1.117	0.09 %
10^4	2.254	2.245	0.40 %
10^5	4.557	4.525	0.70 %
10^6	8.826	8.843	0.19%

The accuracy of the numerical results was verified through numerous tests based on the grid size effect. Since each problem was solved for the two flow regimes using a different code, it was necessary to apply the study of independence of grid to the laminar and turbulent flow code for both the closed cavity and the ventilated cavity, respectively. In the case of natural convection problem (closed cavity), the computational grid that gives grid independent solutions was 91×91 with a maximum deviation of 0.09% and 0.35% for the average Nusselt number for the laminar ($Ra = 10^6$) and for the turbulent regime ($Ra = 10^{12}$), respectively. In the case of mixed convection (ventilated cavity) in laminar and turbulent regime $Ri = 1$, $Ra = 10^6$ and $Ra = 10^{11}$ were used as conditions that may be representative of other situations. In this case, the computational grid that gives grid independent solutions was 111×111 with a maximum deviation of 0.5% for the average Nusselt number in the laminar regime ($Ra = 10^6$), and 5% in the turbulent regime ($Ra = 10^{11}$).

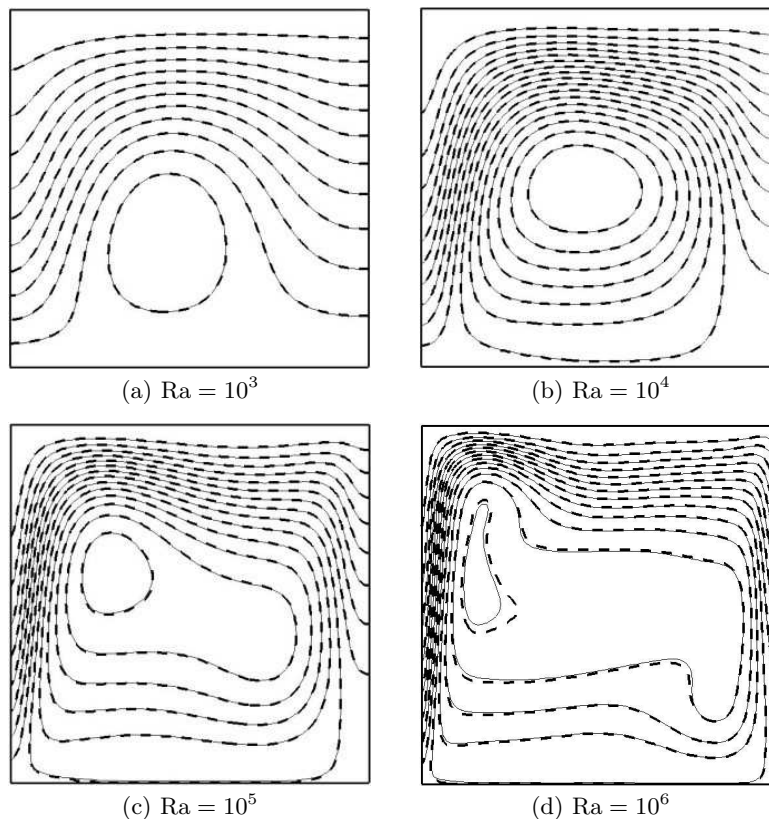


FIG. 3. Qualitative comparison of the dimensionless heatlines obtained from the integration method (dashed line) and the Poisson equation method (continuous line).

5. Results and discussion

For natural convection in the closed cavity, the parameter of study for modeling the heat transfer was the Rayleigh number (Ra), and the Rayleigh and the Richardson number for forced, mixed and natural convection in the ventilated cavity. The dimensions of the cavity were determined from Ra values and are shown in Table 3. The temperatures on the isothermal walls were set as 300 K and 288 K. For the case of the ventilated cavity, the Reynolds number (Re) is a function of the Rayleigh and Richardson numbers from the expression ($Re = [Ra/PrRi]^{1/2}$). The velocity at the inlet of the cavity was determined from Re. Both the U_{in} and the Re for $Ra = 10^3$, 10^6 and 10^9 are presented in Table 4. Air temperature at the inlet is taken as 288 K ($T_{in} = T_C$). The results for the heat function are determined using $T_{ref} = T_C$. The thermal properties were computed at the average temperature T_0 and their values are: $\rho = 1.177 \text{ kg/m}^3$, $\lambda = 26.0\text{E-}03 \text{ W/m} \cdot \text{K}$, $C_p = 1.0\text{E+}03 \text{ J/kg} \cdot \text{K}$, $\beta = 3.322\text{E-}03 \text{ K}^{-1}$ and $\mu = 1.847\text{E-}05 \text{ kg/m} \cdot \text{s}$.

Table 3. Dimensions of the cavity used for the calculations.

Ra (Laminar regime)	L (m)	Ra (Turbulent regime)	L (m)
10^3	9.60E-03	10^9	0.96
10^4	2.07E-02	10^{10}	2.07
10^5	4.46E-02	10^{11}	4.46
10^6	9.60E-02	10^{12}	9.60

Table 4. Reynolds number and inlet velocity for $Ra = 10^3$, 10^6 and 10^9 .

Ra	Ri					
	0.1		1.0		10	
	Re	U_{in}	Re	U_{in}	Re	U_{in}
10^3	118	0.19	37.5	0.06	11.8	0.01
10^6	3750	0.61	1180	0.19	375	0.06
10^9	1.18E+05	1.80	3.75E+04	0.56	1180	0.18

5.1. Closed cavity

The problem was analyzed using the Rayleigh number (Ra) as a reference to cover both laminar and turbulent regime. Figure 4 shows the results for the dimensionless isothermals and heatlines in the laminar flow regime. For different values of Ra, according to the heatlines, the transport of thermal energy occurs

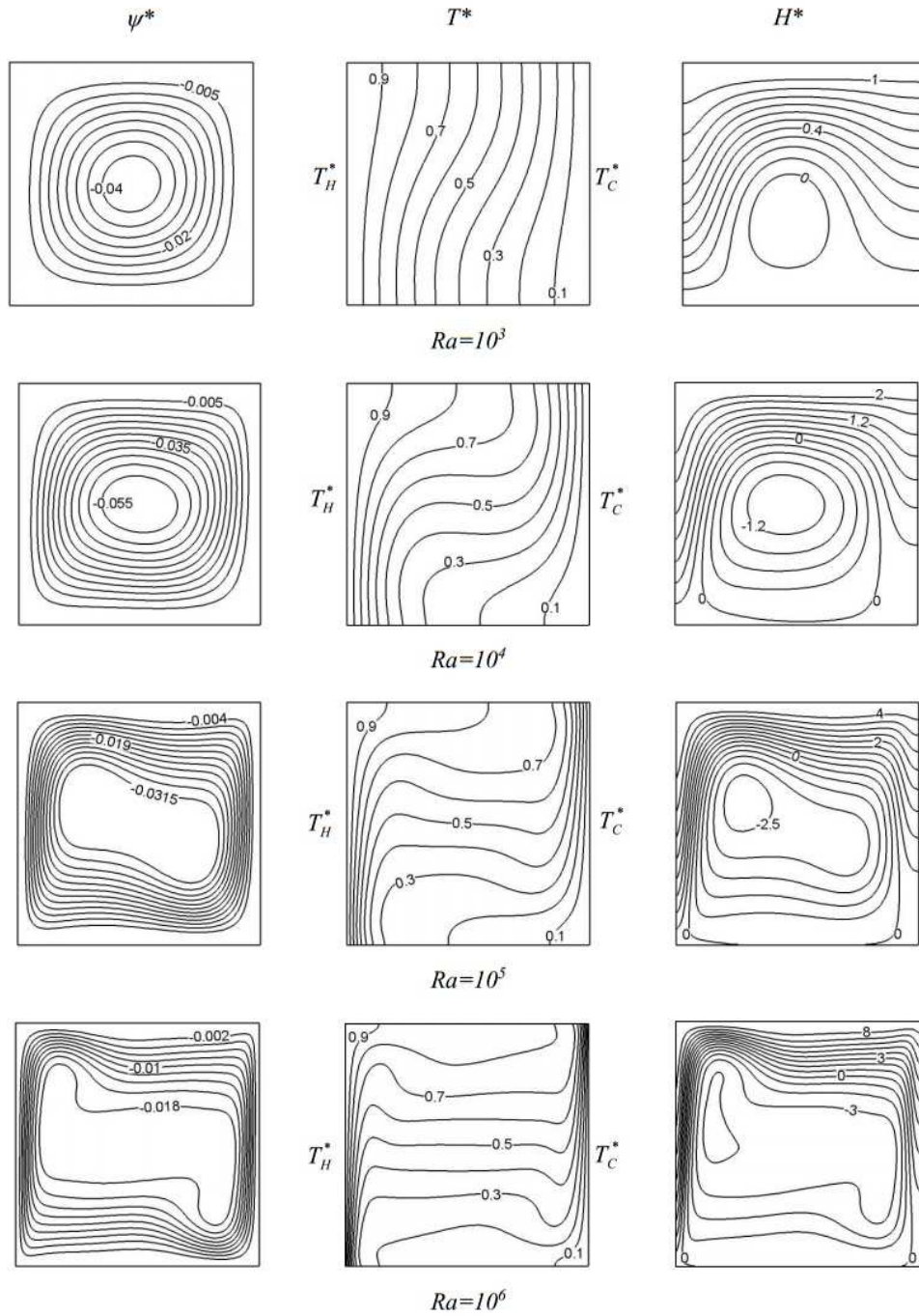


FIG. 4. Dimensionless streamlines, isothermals and heatlines for different Ra in laminar regime.

mainly at the upper zone of the cavity, whereas at the central zone, a recirculation of energy occurs. For a $Ra = 10^3-10^5$, the heatlines emerge perpendicularly from the hot wall on the left boundary, and they reach the cold wall perpendicularly as well. The fluid recirculation at the center of the cavity causes a distortion of the heatlines causing thermal energy to flow from the hot wall to the upper zone of the cavity, being more evident as the Rayleigh number increases. For a $Ra = 10^6$, after emerging from the hot wall, the heatlines become almost parallel in the vicinity of that wall, as an indication that the diffusive process is increasingly confined to the isothermal walls, whereas the advective transport becomes stronger at the center of the cavity.

For the turbulent regime, Fig. 5 shows that the heatlines exhibit a pattern similar to the streamlines, whereas they are parallel to the isothermals in most part of the cavity. This is because of higher values of Rayleigh, the temperature gradients are more intense at the boundary layer, and become almost zero at the center of the cavity. This way, the energy transport depends mostly on the fluid flow. This is the main cause of the similarity between the streamlines and the heatlines; nevertheless, the heatlines are not as symmetric as the streamlines, that is to say, there is an equal number of streamlines on the upper side of the cavity than on the lower side, as an indication that the fluid recirculates completely inside the cavity. However, there is an increased number of heatlines on the upper side of the cavity in comparison to the lower side. This can be interpreted as an indication that the energy transfers from the hot wall to the cold wall over the upper side; this situation cannot be explained through the isothermals.

Figures 6 and 7 show the behavior of the dimensionless heat function, temperature and velocities at the center of the cavity all along $x^* = 0.5$ and $y^* = 0.5$ for the laminar and turbulent flow regime, respectively. It can be observed that for all the cases, negative values of the heat function are present below the region close to $y^* = 0.8$. These values indicate that thermal energy recirculation is present. After this region, the heat function grows until it reaches its maximum value, which in all the cases occurs at $y^* = 1.0$, indicating that the thermal energy transfer is carried out mainly at the upper side of the cavity; this behavior occurs because the hot fluid flows in this region once it has moved from the region adjacent to the hot wall. Moreover, along $y^* = 0.5$ the heat function shows a parabolic profile, which indicates that more intense gradients for the heat function are at the regions close to the isothermal walls. In addition, the gradients for the heat function are null within the region $0.1 < x^* < 0.9$, as an indication that the energy flow in that zone is minimum due to the stratification of the fluid. This stratification can be observed in the temperature and the vertical velocity in Figs. 6b, 6c, 7b and 7c. For $Ra < 10^6$, the Rayleigh number has a strong effect on the heat function, temperature and vertical velocity profiles.

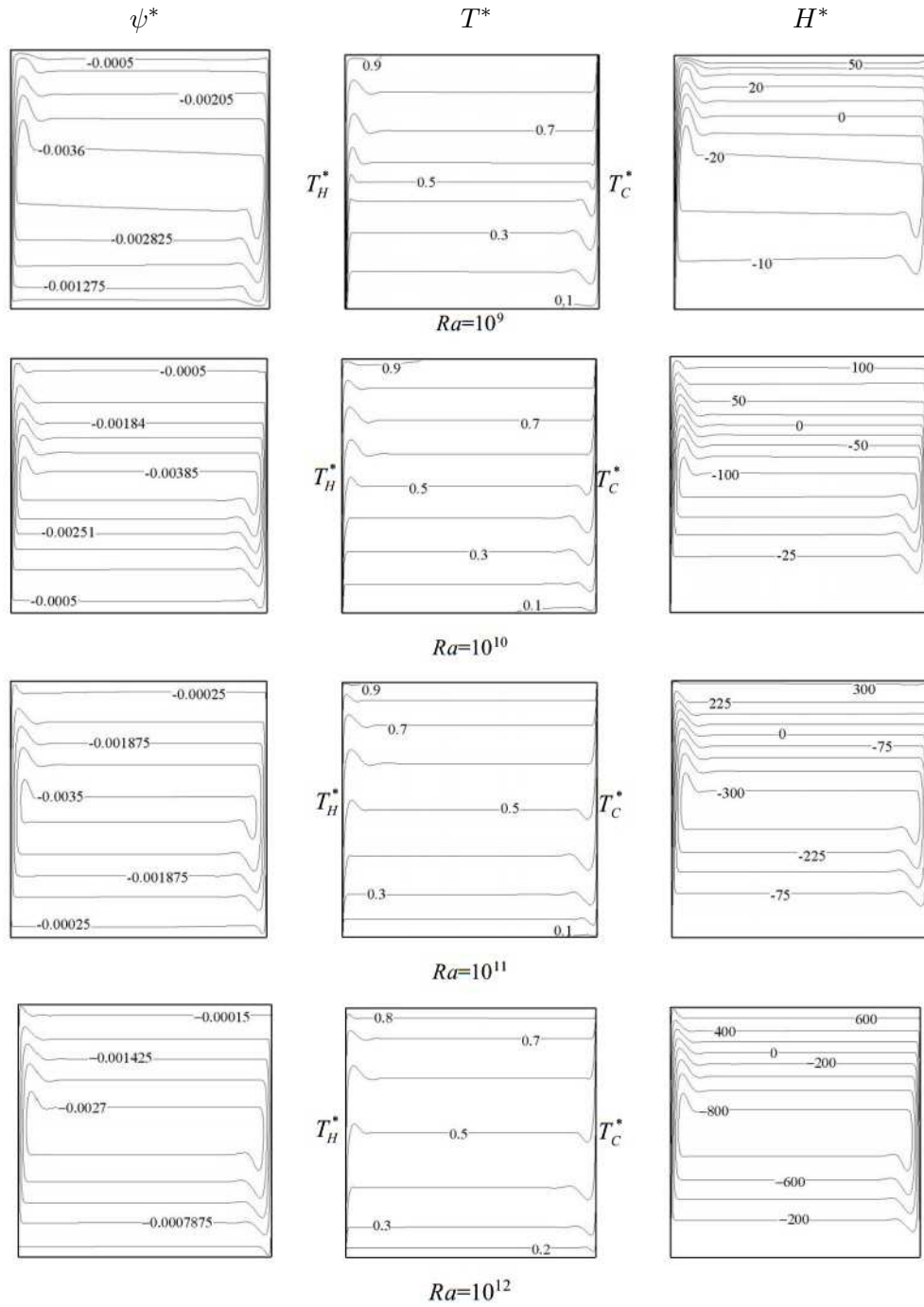


FIG. 5. Dimensionless streamlines, isothermals and heatlines for different Ra in turbulent regime.

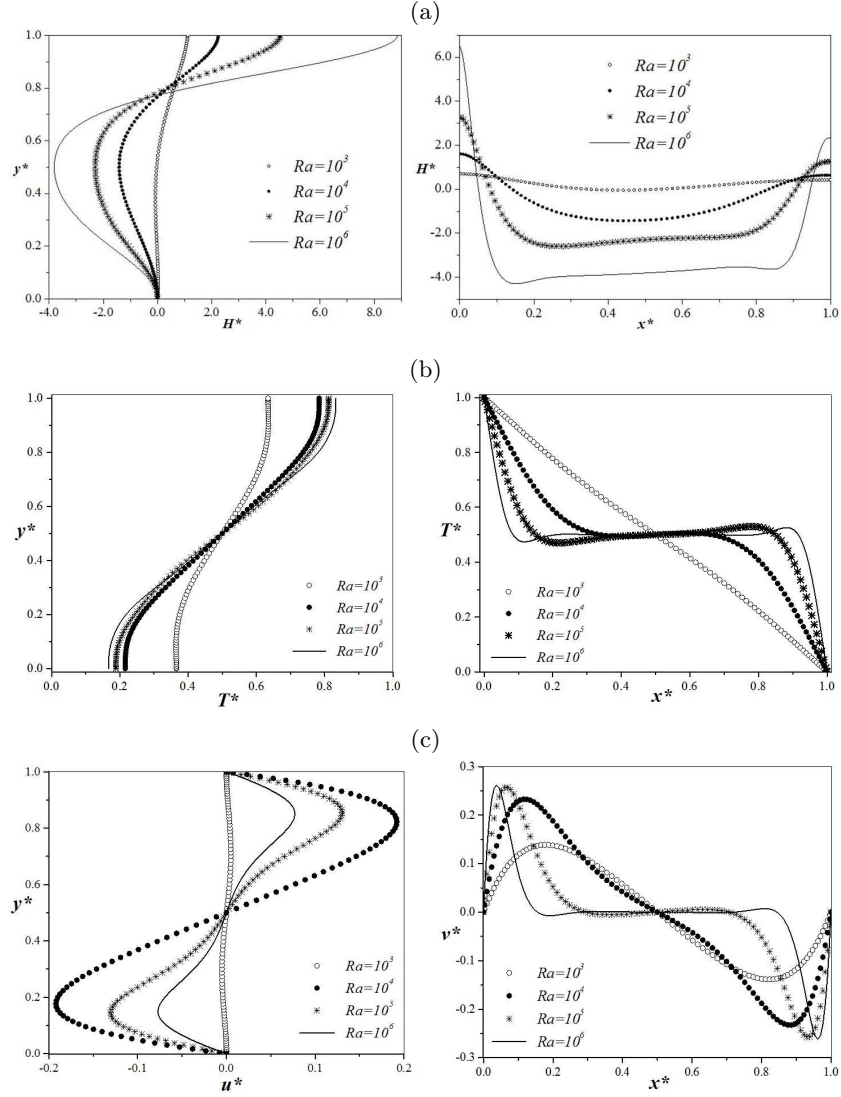


FIG. 6. Behaviour of the dimensionless heat function, temperature and velocities along the coordinate $x^* = 0.5$ (left) and the coordinate $y^* = 0.5$ (right) for $Ra = 10^5$.

Nevertheless, for $Ra > 10^9$ there is no appreciable effect neither on temperature nor vertical velocity, but the effect is noticeable for the heat function. This effect may be due to the recirculation of fluid in the core of the cavity. This recirculation is influenced by the horizontal velocity and the temperature as can be seen in the profiles along $x^* = 0.5$ (Figs. 7b and 7c). Besides, as the Ra increases this recirculation becomes stronger, which makes more evident the increment on the dependency of the advective effect.

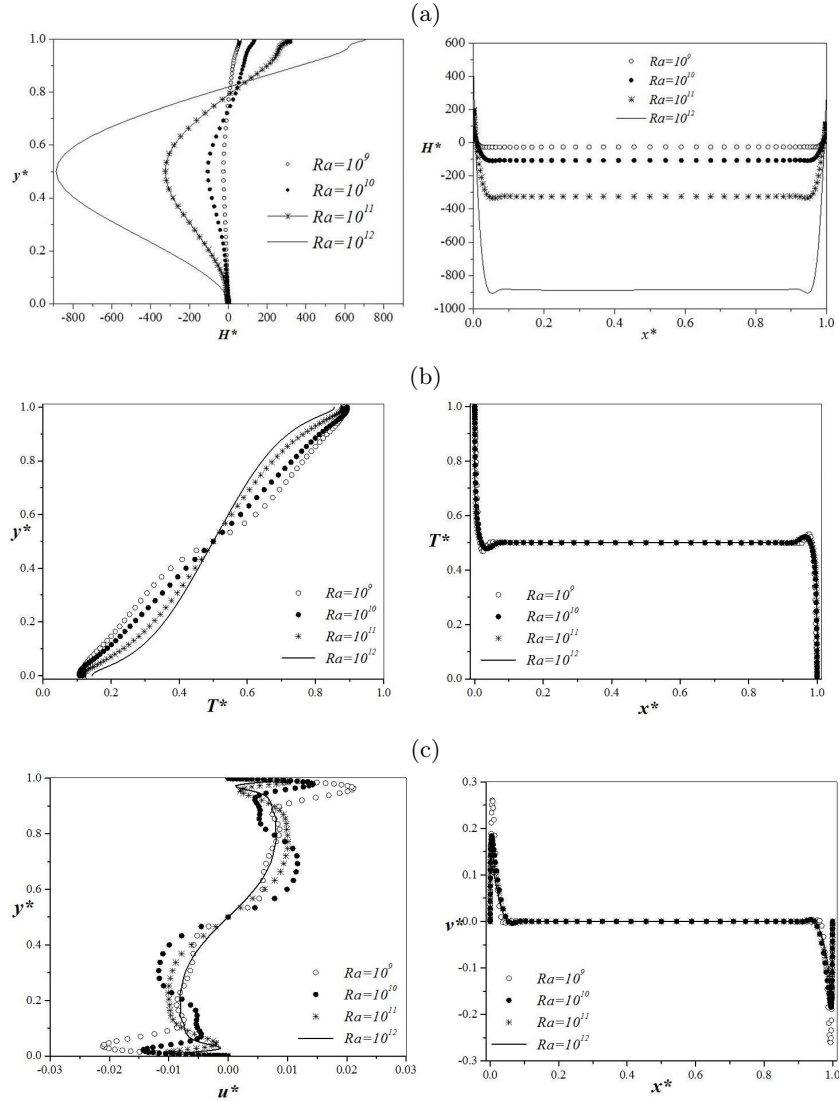


FIG. 7. Behaviour of the dimensionless heat function, temperature and velocities along the coordinate $x^* = 0.5$ (left) and the coordinate $y^* = 0.5$ (right) for $Ra = 10^9$.

5.2. Ventilated cavity

Figures 8–11 show the flow patterns for different Rayleigh numbers (10^3 , 10^5 , 10^9 and 10^{11}) and for each Richardson number considered in this study (0.1, 1 and 10).

For the case of $Ra = 10^3$ (Fig. 8) the heatlines show that the heat diffusion process occurs in most of the cavity. For $Ri = 0.1$ it can be observed that the

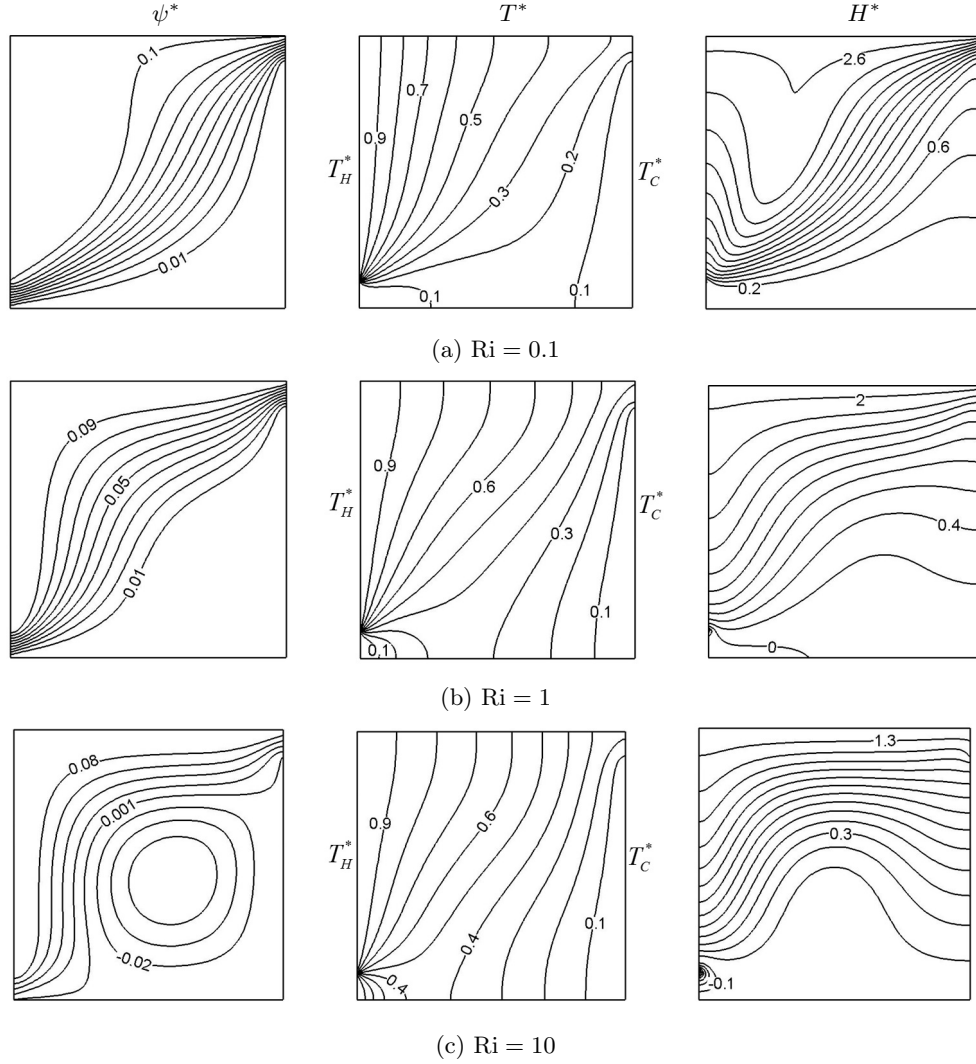


FIG. 8. Dimensionless streamlines, isothermals and heatlines for $Ra = 10^3$: (a) $Ri = 0.1$, (b) $Ri = 1$ and (c) $Ri = 10$.

energy flow starts at the hot wall and suddenly changes its path because the air flow transports energy to the cold wall, becoming more intense at the air outlet. Instead, for $Ri = 1$ the heat flux starts at the hot wall, causing the energy flow to be present in most of the cavity, as shown by the heatlines. For $Ri = 10$ the heatlines pattern is very similar to the mixed convection case, but unlike the first case, the heatlines show a slight perturbation at the center of the cavity due to the recirculation of the fluid in this area. Besides, the heatlines show that there is a small energy flow going from the lower side of the hot wall to

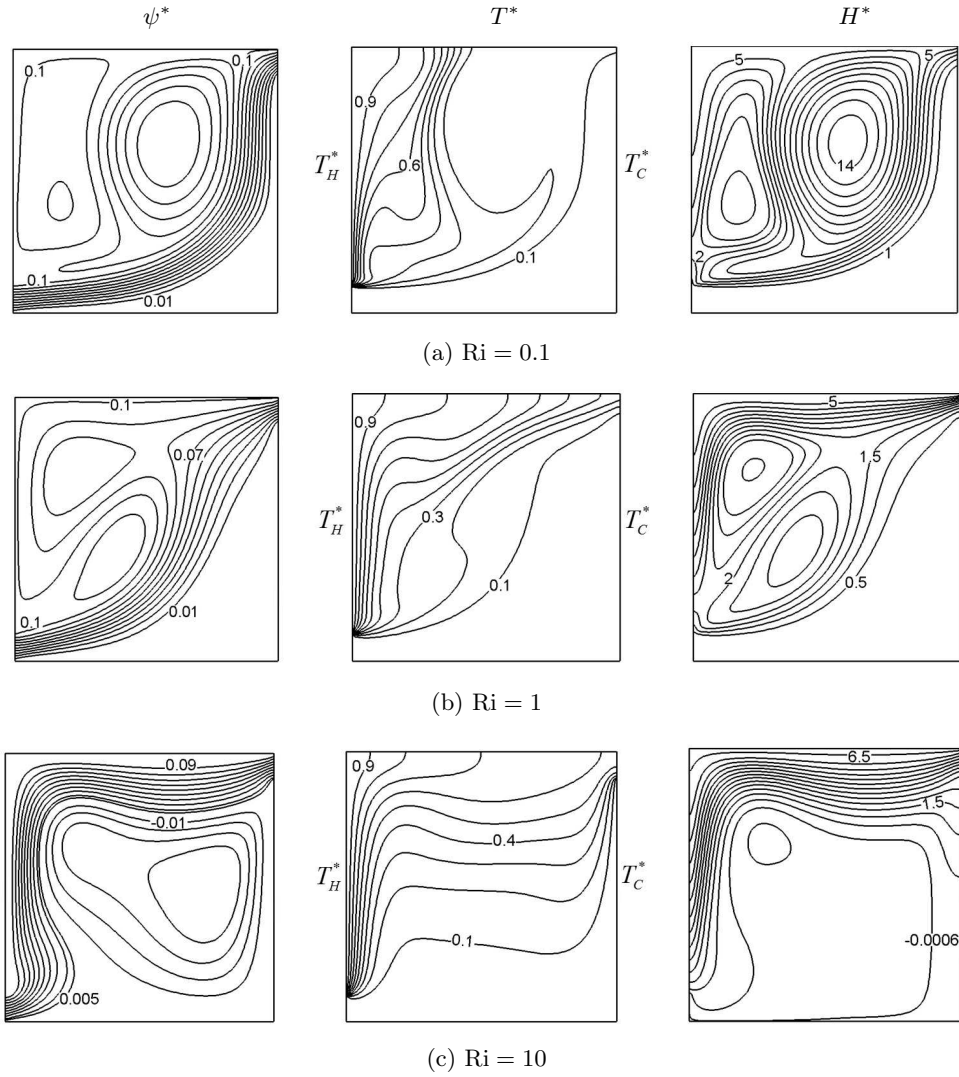


FIG. 9. Dimensionless streamlines, isothermals and heatlines for $Ra = 10^5$: (a) $Ri = 0.1$, (b) $Ri = 1$ and (c) $Ri = 10$.

the air inlet. The energy flow goes opposite to the fluid flow because the energy transport in this region is mainly by diffusion, this phenomenon can be observed only through the heatlines. In Fig. 9, it is shown that for $Ra = 10^5$ the heatlines reveal that the energy transport is mostly due to the advective process. This way, the heatlines are very similar to the streamlines in most of the cavity. Moreover, the diffusive process is limited to the regions close to the isothermal walls. It can be observed that for $Ri = 0.1$ and $Ri = 10$ the maximum values are achieved for the heatlines of 14 and 6.5 respectively, indicating that forced convection

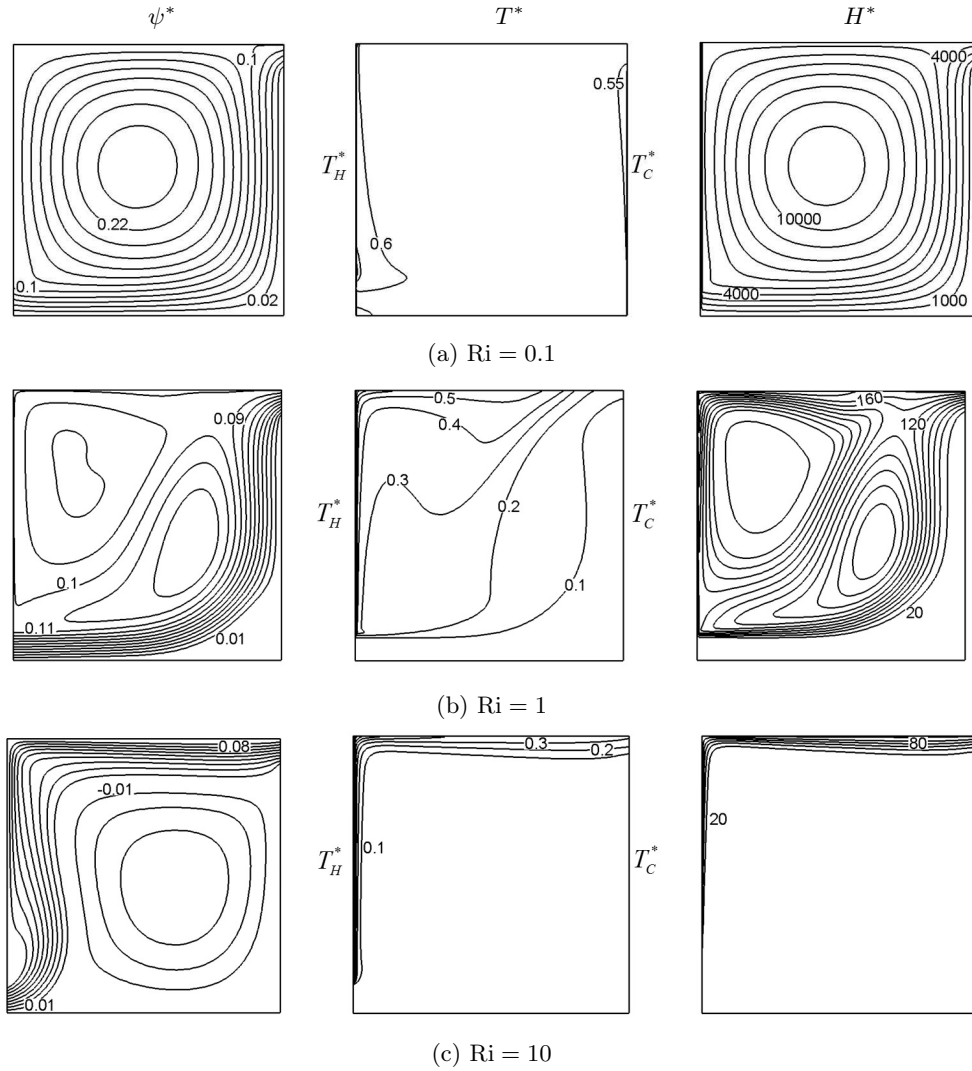


FIG. 10. Dimensionless streamlines, isotherms and heatlines for $Ra = 10^9$: (a) $Ri = 0.1$, (b) $Ri = 1$ and (c) $Ri = 10$.

is better for transporting the thermal energy in the cavity. This effect is very strong for $Ra = 10^6$, where the maximum values for the heatlines are 55 and 12 for $Ri = 0.1$ and $Ri = 10$, respectively.

In Figs. 10–11, it is shown that for $Ra = 10^9$ and 10^{11} the flow patterns indicate that the heat transfer is due to the energy advection. This way, heat diffusion is confined to the boundary layer. It can be observed that for $Ri = 0.1$, the heatlines and streamlines patterns are very similar, with the only difference that the first ones emerge from the hot wall, while the last ones emerge from the

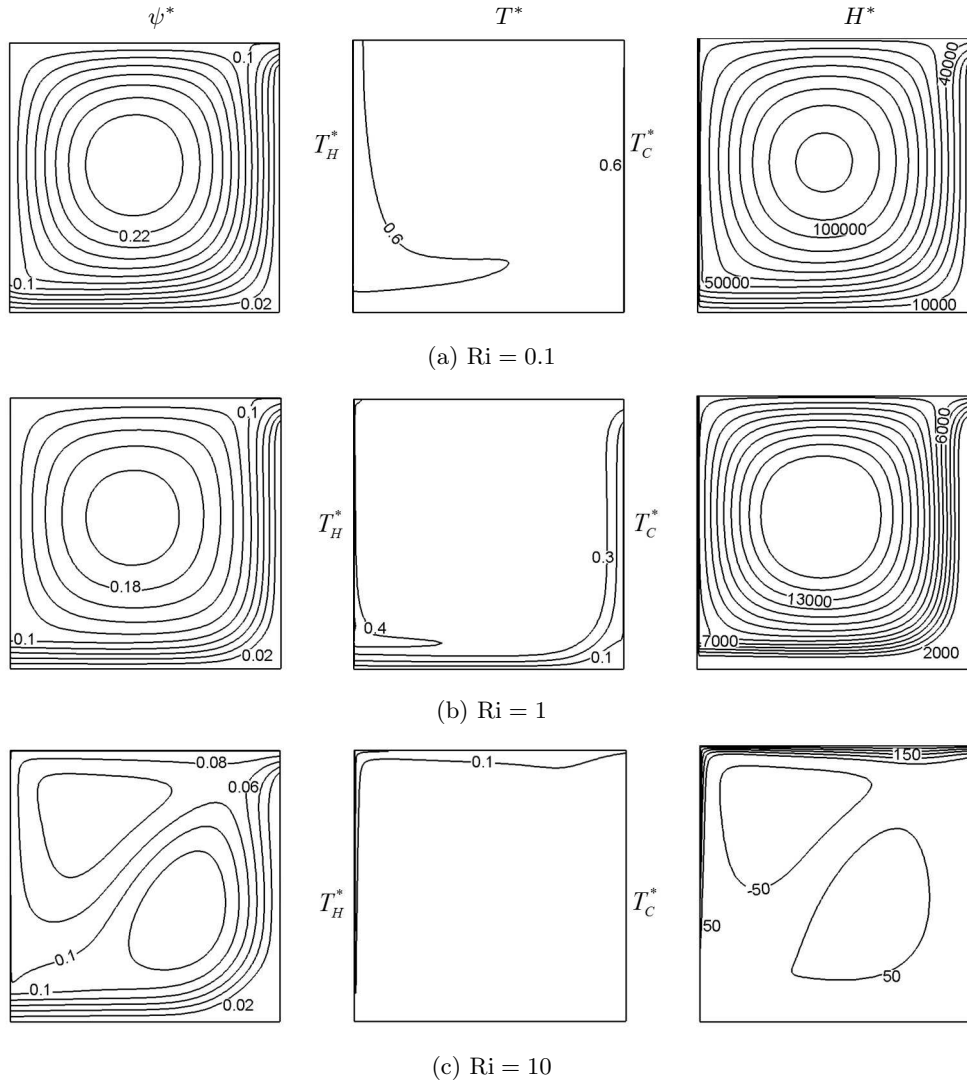


FIG. 11. Dimensionless streamlines, isotherms and heatlines for $Ra = 10^{11}$: (a) $Ri = 0.1$, (b) $Ri = 1$ and (c) $Ri = 10$.

fluid inlet. For $Ri = 10$, the thermal energy transport is carried out through the top of the cavity. On the other hand, for $Ri = 1$ the heatlines show a separation of the energy flow; a fraction of this energy is transported through the upper side of the cavity, while the other one is transported through the lower side, meeting each other at the air outlet. However, heatlines indicate that this separation is broken when the Ra is greater than 10^9 making the energy transport the same as in the case of $Ri = 0.1$.

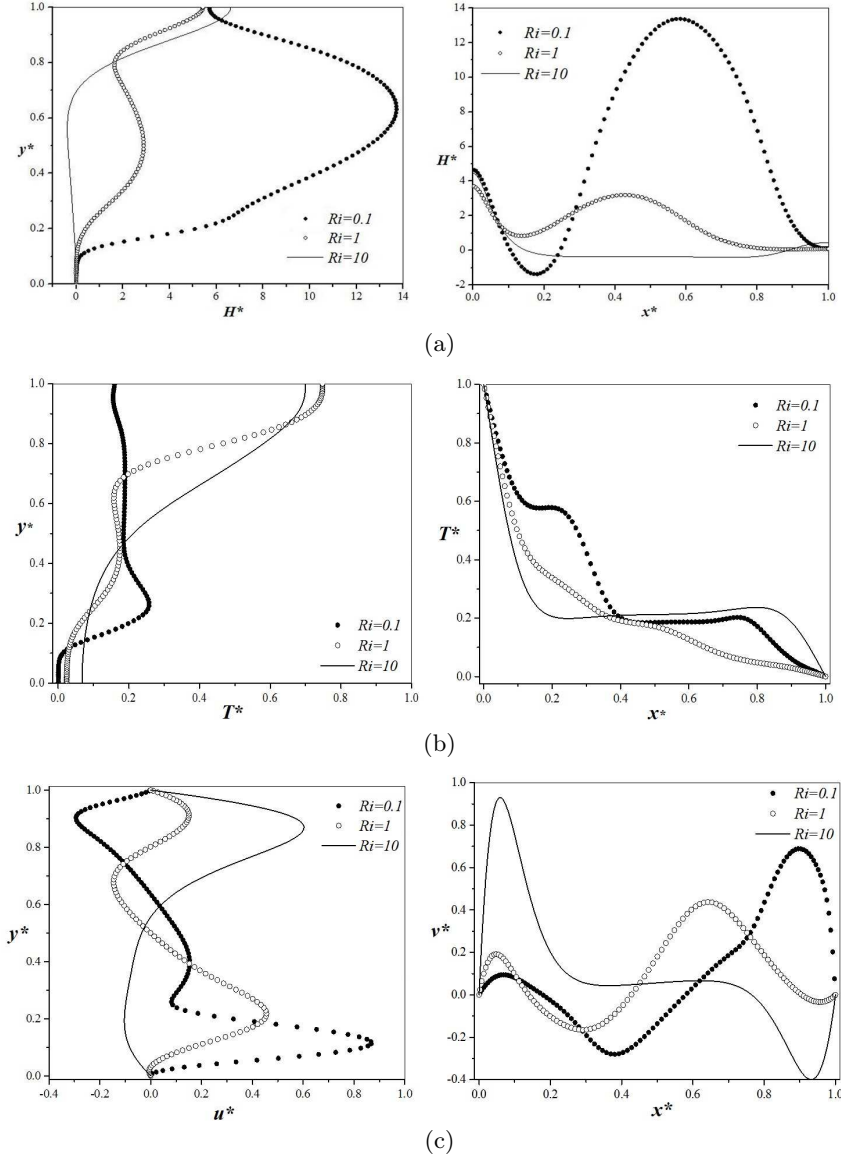


FIG. 12. Behaviour of the dimensionless (a) heat function, (b) temperature and (c) velocities along the coordinate $x^* = 0.5$ (left) and the coordinate $y^* = 0.5$ (right) for $Ra = 10^5$.

Finally, the heat function, temperature and velocity profiles at the center of the cavity for the cases $Ra = 10^5$ and $Ra = 10^9$ are shown in Figs. 12 and 13, respectively. For $Ra = 10^5$, the heatline profile has a parabolic behavior when the $Ri = 0.1$, showing that there is a high level of energy recirculation. For $Ri = 0$ and $Ri = 10$, the major changes on the heatline are an indication that the thermal

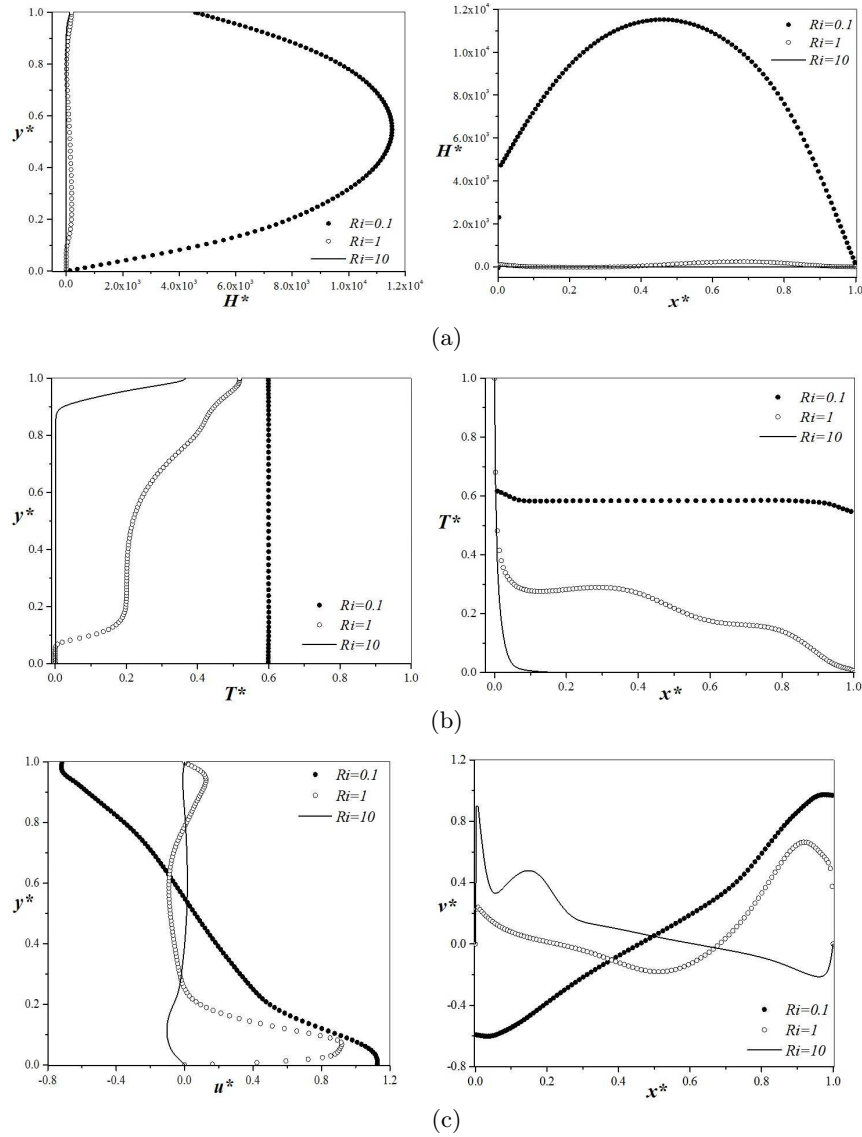


FIG. 13. Behaviour of the dimensionless: (a) heat function, (b) temperature and (c) velocities along the coordinate $x^* = 0.5$ (left) and the coordinate $y^* = 0.5$ (right) for $Ra = 10^9$.

flow occurs at the highest part of the cavity, along the adjacent region of the hot wall. Regarding natural convection, thermal energy is dragged in a similar way as the closed cavity, i.e., the buoyant forces drive the energy between the region $y^* = 0.8$ and $y^* = 1.0$. In the case of $Ra = 10^9$, the heat function profiles indicate that the thermal energy transport is greater than when $Ri = 0.1$. As

the Ri increases, the numerical value of the heat function and the temperature drops abruptly. For $Ri = 0.1$, the temperature is constant and homogenized in the cavity at $T^* = 0.6$, as it is seen in Fig. 13b. Additionally, Fig. 13c allows to observe that velocity profiles are quite different from each other. The profiles for $Ri = 0.1$ are the biggest, while the profiles for $Ri = 10$ are the smallest. The velocity profiles for $Ri = 1$ have characteristics of the other ones, they have high values in the lowest part and near the hot wall like in the cases when $Ri = 0.1$ and $Ri = 10$, respectively. However, temperature is very different for each case. The difference between the temperature and velocity profiles is the main reason that the energy transport is different. For $Ri = 1$ and $Ri = 10$, it can be observed that the behavior of the heat function is very similar and almost constant, i.e., heat transfer by mixed and natural convection has the same order of magnitude, whereas in forced convection it is greater. This is a consequence of the inertia of the fluid due to the inlet velocity. The results allow to see that forced convection tends to homogenize the temperature of the cavity to a value near the average of the isothermal walls, while natural convection has the same behavior to the value of $Ri = 0.1$. This fact may help in making a decision when ventilation or heating is required, e.g., if the inlet temperature is the comfort temperature, natural convection is preferred for ventilation, whereas, if heating is required, forced convection is the choice.

6. Conclusions

The heatline concept has been used to visualize and interpret the result of problems on (1) natural convective heat transfer in a closed differentially heated cavity and (2) forced, mixed and natural convective heat transfer in a ventilated differentially heated cavity. The calculations were carried out for laminar and turbulent regime flows, and regarding the ventilated cavity three cases of convection defined by $Ri = 0.1$, 1.0 and 10 were studied.

Based on the obtained results it can be concluded that:

1. In the closed cavity with natural heat convection, the isothermals are very useful for analysis purposes when Ra is under 10^3 , as shown by the heatlines; the energy flow is almost perpendicular to the isothermals. Nevertheless, as Ra increases, the heatlines begin to look like the streamlines. Thereby, it is possible to estimate the path of the thermal energy using the streamlines when the Ra is high, especially in the turbulent regime. In addition, the heatlines let us visualize that the transport of thermal energy is always performed through the top of the cavity.

2. The interaction of the buoyancy and the inertial forces play an important role in the path of the energy. Unlike the case of the closed cavity, in the ventilated cavity the transport of thermal energy is not always performed along the

top of the cavity. There are three possible situations for the thermal energy flow: (i) it is dragged by the incoming fluid from the hot wall to the outlet when the inertial force is greater than the buoyant one ($Ri = 0.1$), (ii) it is carried by the buoyant force through the top of the cavity when $Ri = 10$ and (iii) the transport of the thermal energy is dragged by both the buoyancy force and the inertial force ($Ri = 1.0$). In the laminar regime, it is found that the path of the energy flow is independent of Ra . In the turbulent regime when $Ri = 0.1$ and 10 , the path of the energy flow is also independent. However, for $Ri = 1.0$ the separation of the energy flow changes its pattern when Ra is greater than 10^9 .

3. The order of magnitude of the heatline profiles shows that the transport of thermal energy for $Ri = 0.1$ is higher than for $Ri = 1.0$ and $Ri = 10$. This effect is due to the advective component for $Ri = 0.1$ (forced convection); it is higher than the advective component for $Ri = 1.0$ and 10 (mixed and natural convection). In addition, such an effect is stronger in the turbulent regime than in the laminar regime.

4. For the ventilated system, the use of heat lines in conjunction with the temperature and velocity profiles allows to see that natural convection is preferred when cooling is required, while the forced convection is a better choice if heating is needed.

7. Acknowledgement

The authors are grateful to the Consejo Nacional de Ciencia y Tecnología (CONACYT), whose financial support made this work possible.

References

1. S. KIMURA, A. BEJAN, *The heatline visualization of convective heat transfer*, ASME Journal of Heat Transfer, **105**, 916–919, 1983.
2. S.K. AGGARWAL, A. MANHAPRA, *Use of heatlines for unsteady buoyancy-driven flow in a cylindrical enclosure*, ASME Journal of Heat Transfer, **111**, 576–578, 1989.
3. F.Y. ZHAO, D. LIU, G.F. TANG, *Application issues of the streamline, heatline and massline for conjugated heat and mass transfer*, International Journal of Heat and Mass Transfer, **50**, 320–334, 2007.
4. P. BISWAL, T. BASAK, *Sensitivity of heatfunction boundary conditions on invariance of Bejan's heatlines for natural convection in enclosures with various wall heatings*, International Journal of Heat and Mass Transfer, **89**, 1342–1368, 2015.
5. F.L. BELLO-OCHEDE, *A heat function formulation for thermal convection in a square cavity*, International Communications in Heat and Mass Transfer, **15**, 193–202, 1988.
6. W.A. WAHEED, *Temperature dependent fluid properties effects on the heat function formulation of natural convective flow and heat transfer*, International Journal of Numerical Methods in Heat and Fluid Flow, **16**, 240–260, 2006.

7. Q.H. DENG, *Fluid flow and heat transfer characteristics of natural convection in square cavities due to discrete source-sink pairs*, International Journal of Heat and Mass Transfer, **51**, 5949–5957, 2008.
8. M. MOBEDI, U. ÖZKOL, B. SUDEN, *Visualization of diffusion and convection heat transport in a square cavity with natural convection*, International Journal of Heat and Mass Transfer, **53**, 99–109, 2010.
9. Q.H. DENG, G.F. TANG, *Numerical visualization of mass and heat transport for mixed convective heat transfer by streamline and heatline*, International Journal of Heat and Mass Transfer, **45**, 2387–2396, 2002.
10. D. RAMAKRISHNA, T. BASAK, S. ROY, I. POP, *A complete heatline analysis on mixed convection within a square cavity: effects of the thermal boundary conditions via thermal aspect ratio*, International Journal of Thermal Sciences, **57**, 98–111, 2012.
11. T.Y. KIM, S.W. BAEK, *Analysis of combined conductive and radiative heat transfer in a two-dimensional rectangular enclosure using the discrete ordinates method*, International Journal of Heat and Mass Transfer, **34**, 2265–2273, 1991.
12. Q.H. DENG, G.F. TANG, *Numerical visualization of mass and heat transport for conjugate natural convection/heat conduction by streamline and heatline*, International Journal of Heat and Mass Transfer, **45**, 2373–2385, 2002.
13. M. MOBEDI, *Conjugate natural convection in a square cavity with finite thickness horizontal wall*, International Communications in Heat and Mass Transfer, **35**, 503–513, 2008.
14. S.K. DASH, *Heatline visualization in turbulent flow*, International Journal of Numerical Methods in Fluid Flow, **5**, 37–46, 1996.
15. G. DELIBRA, K. HANJALIC, D. BORELLO, F. RISPOLI, *Vortex structures and heat transfer in a wall-bounded pin matrix: LES with a RANS wall-treatment*, International Journal of Heat and Fluid Flow, **31**, 740–753, 2010.
16. R. HENKES, F. VAN-DER-VLUGT, C. HOOGENDOORN, *Natural-convection flow in a square cavity calculated with low-Reynolds-number turbulence models*, International Journal of Heat and Mass Transfer, **34**, 377–388, 1991.
17. I. HERNÁNDEZ-LÓPEZ, *Líneas de calor: visualización y análisis en problemas de transferencia de calor por convección en cavidades rectangulares (Heatlines: visualization and analysis of convection heat transfer problems in rectangular cavities)*, Cenidet, Cuernavaca Morelos, México, 2010.
18. I. HERNÁNDEZ-LÓPEZ, *Análisis de la transferencia de calor conjugada en un sistema solar pasivo de muro Trombe para calentamiento o ventilación (Analysis of the conjugate heat transfer in a solar passive system of Trombe wall for heating or ventilation)*, Cenidet, Cuernavaca Morelos, México, in process 2015.
19. S.V. PATANKAR, *Numerical Heat Transfer and Fluid Flow*, Hemisphere Publishing Corporation, New York 1980.
20. J.P. VAN DOORMAAL, G.D. RAITBY, *Enhancements of the SIMPLE method for predicting incompressible fluid flows*, Numerical Heat Transfer, **7**, 147–163, 1984.
21. G. DE VAHL DAVIS, *Natural convection of air in a square cavity a benchmark numerical solution*, International Journal of Numerical Methods in Fluids, **3**, 249–264, 1983.

-
22. T. FUSEGI, J. HYUN, K. KUWAHARA, *Tree-dimensional simulations of natural convection in sidewall-heated cube*, International Journal of Numerical Methods in Fluids, **3**, 857–867, 1991.
 23. N. MARKATOS, K. PERICLEUS, *Laminar and turbulent natural convection in an enclosed cavity*, International Journal of Heat and Mass Transfer, **27**, 755–772, 1984.
 24. G. BARAKOS, E. MITSOULIS, D. ASSIMACOPOULOS, *Natural convection flow in a square cavity revisited: laminar and turbulent models with wall functions*, International Journal of Numerical Methods in Fluids, **18**, 695–719, 1994.

Received January 27, 2015; revised version August 11, 2015.
